7-26-1986

Beam Voltage Effects in the Study of Embedded Biological Materials by Secondary Electron Detectors

C. Scala
University of Bologna

G. Pasquinelli
University of Bologna

P. Preda
University of Bologna

R. Laschi
University of Bologna

Recommended Citation

Utah State University
MERRILL-CAZIER LIBRARY

BEAM VOLTAGE EFFECTS IN THE STUDY OF EMBEDDED BIOLOGICAL MATERIALS
BY SECONDARY ELECTRON DETECTORS

C. Scala, G. Pasquinelli, P. Preda, R. Laschi[*]

Institute of Clinical Electron Microscopy,
University of Bologna and Institute of Normal
and Pathological Cytomorphology, CNR, Italy

Abstract

Thin and semithin sections were extensively examined by the secondary electron (SE) detector in a conventional scanning electron microscope (SEM), and in a transmission electron microscope with a scanning attachment (STEM). Various parameters, in particular the beam voltage, were shown to affect the final SE image (SEI). As for SEM observation, a surface contrast was imaged at low primary electron (PE) voltages (0.6-2 kV), whereas a subsurface contrast predominated at higher energies (15-30 kV). In STEM, significant differences were not detected by varying the PE in the 20-100 kV range. Surface and subsurface information was simultaneously imaged even though the SEI were better resolved at the highest energy.

*Address for correspondence: R. Laschi
Director of Institute of Clinical Electron
Microscopy, University of Bologna,
Via Massarenti 9 - 40138 Bologna, Italy.
Phone No. 051 302874

Introduction

In electron microscopy all information obtained from a specimen has its origin in the electron beam-specimen interaction. Modification of the electron beam or radiation produced by this interaction can be interpreted as specimen structure or topography (transmitted electrons, secondary electrons) and composition (backscattered electrons, X-ray photons).

Whatever the signals are, they can be collected in a scanning electron microscope (SEM) by using different detectors thus providing well contrasted images. The most common and widely used detector in scanning electron microscopy is the Everhart-Thornley scintillator/photomultiplier secondary electron detector (SED) (Everhart et al., 1959; Everhart and Thornley, 1960). The SED collects predominantly those electrons with energies varying from 0 to 50 eV which are conventionally named secondary electrons (SE). As the conventional theory postulates (Oatley et al., 1965; Drescher et al., 1970; Reimer, 1979; Peters, 1982b; Hasselbach et al., 1983; Pawley, 1984), SE are produced at least by four mechanisms:

Type I: interaction of the primary electron beam (PE) with the specimen surface near the point of entry;

Type II: interaction of high energy backscattered electrons (BSE) generated below the surface, as they re-emerge through the surface at some distance from the entry point;

Type III: interaction between these same BSE and the walls of the specimen chamber, mainly the lower surface of the final lens pole piece;

Type IV: interaction between the PE and the microscope apertures.

Of these mechanisms, only the first is expected to give high resolution surface information related to the impact point of the beam against the specimen surface because of the very short range of these SE (Pawley, 1984; Joy, 1985).

The other two types of interaction (SE-II, SE-III) contribute to give subsurface delocalized information as these SE are produced by BSE coming from some microns below the specimen surface. The SE-IV gives a limited contribution to the final SE image (2-10% of the total SE signal, Joy, 1984). This unwanted contribution reduces the signal contrast and can be minimized by placing the final aperture before the probe forming lens (Peters, 1982b; Peters, 1983).

The final SE image (SEI) is formed by a combination of all the detected SE and of those BSE which are emitted towards the SED (Reimer et al., 1968; Drescher et al., 1970; Peters, 1982b; Volbert, 1982). This BSE signal, as a result of high angle elastic scattering events, is composed of BSE which re-emerge from both the PE entry (BSE-I) and at some distance from it (BSE-II) (Drescher et al., 1970; Niedrig, 1978; Peters, 1982b). As a consequence of the conventional theory, both surface topographical and compositional subsurface contrasts, obtained from a specimen conventionally processed for SEM (dehydrated and covered with a thin layer of conductive elements), are widely BSE dependent.

In the last few years, some authors have begun to study paraffin and plastic embedded sections by means of BSE detectors for correlating optical and ultrastructural observations (DeNee et al., 1977; Kushida et al., 1977; Dichiara et al.,1980; Ogura and Hasegawa, 1980; Ogura and Laudate, 1980; Hartman and Nakane, 1981). The advantage of using specimens with minimal surface morphology is to collect mainly the compositional component of the signal detected by the BSE detector. In this way it is possible to obtain some information related to high Z areas of specifically stained sections (compositional BSE).

In our previous papers (Pasquinelli et al., 1985; Scala et al., 1985) we tested the conventional SED on thin and semithin plastic embedded biological sections. Some variables affecting the final SEI were considered. In particular, the signal collected by the SED was influenced by: instrumental parameters (design of the specimen chamber and collection geometries of the SED) which are usually not under the operator's control; operating conditions, such as beam spot size, PE voltage, working distance and tilt of the specimen stub with respect to the SED location, which can be modified; specimen processing conditions and, in particular, the thickness and the atomic composition (Z) of the sections examined.

As for the instrumental parameters, the data obtained by using two different collection geometries of SED (bottom SED, top SED) were extremely interesting. The images obtained in SE and BSE mode by bottom SED are, in fact, similar, whereas the same images by top SED were fully diversified. The operating conditions seemed to be more or less critical: beam spot size, working distance and tilt influence mainly the final image resolution and the yield of the signal collected; PE voltage allows the diversification of surface and subsurface information.

The thickness and the atomic composition of the section (mean Z constitution, presence of surface high Z particles, etc) contribute to characterize the information depth within the specimen.

From our results, it seems clear that a further characterization of the effects of different PE voltages on sections varying in thickness, was necessary to evaluate the possibility of obtaining information from different layers of the same specimen. For this reason, thin and semithin sections of plastic embedded material, conventionally stained (uranyl acetate and lead citrate) and/or subjected to cytochemical and immunocytochemical procedures, were studied by a bottom SED in a SEM (PE ranging from 0.6 to 30 kV) and by a top SED in a STEM (PE ranging from 20 to 100 kV).

Materials and Methods

Thin and semithin sections of human material were conventionally stained (uranyl acetate and lead citrate) and/or subjected to cytochemical and immunocytochemical procedures thus permitting a correlation between SE, TE and BSE images (SEI, TEI and BEI).

Carotid

Small fragments were fixed in 2.5% glutaraldehyde in cacodylate buffer, pH 7.2-7.4 with 3 mg/ml tannic acid for two hours (Cotta-Pereira et al., 1976), washed in cacodylate buffer 0.1 M and postfixed in 1% osmium tetroxide in Veronal acetate buffer. The fragments were dehydrated by means of a graded acetone series and embedded in Araldite. Thin (80 nm) and semithin section (0.5-1 μm), cut with LKB Ultrotome IV, were counterstained with uranyl acetate and lead citrate.

Myocardium

Myocardium slices were fixed in 2% glutaraldehyde-2% paraformaldehyde in Sorensen's phosphate buffer, dehydrated through an ethanol series, cleared in propylene oxide and embedded in Araldite. The protein A-gold immunocytochemical technique (Roth et al., 1978) was applied on thin sections for the detection of actin. The sections were stained with uranyl acetate and

lead citrate.
Small intestine
Samples were fixed in periodate-lysine-para-formaldehyde (McLean and Nakane, 1974), dehydrated and embedded as above. The protein A-gold immunocytochemical technique (Roth et al., 1978) was applied on semithin sections for the detection of actin. Labelling was enhanced by a silver precipitation reaction in some specimens (Danscher and Nörgaard, 1983).
Kidney
Kidney slices were fixed in 2.5% glutaraldehyde in Sorensen's phosphate buffer, postfixed in 1% osmium tetroxide in Veronal acetate buffer, dehydrated and embedded as above. Thin and semithin sections were stained with uranyl acetate and lead citrate.

The preparation of sections was carried out as follows: thin sections (80 nm) were collected on nickel grids and covered with 20 nm of evaporated pure carbon and observed by SED and TE detector (TED); semithin sections (0.5-1 μm) were mounted as above or on glass slides, successively cut into small pieces (1x1 cm), glued on stubs and covered, under vacuum, with 20 nm of carbon for examination in SE and BSE mode.

Instruments and operating parameters.
Specimens of different thicknesses (ST) were observed by SEM (Philips 515) fitted with a LaB$_6$ cathode, in different conditions. Primary electron voltages (PE): ranging from 0.6 to 30 kV; beam spot size (S): 20 nm; specimen stage tilt (Tilt): 15°; working distance: eucentric high (EH, 12 mm) position.

In addition, some specimens were observed by a Philips 400T (TEM) fitted with a scanning attachment, operating at PE from 20 to 100 kV; S from 5 to 20 nm; tilt of 15°.

The same contrast and the same printing conditions were used in all micrographs obtained (TEI, SEI and BEI). In some images the negative polarity mode (indicated by (-)) was used in order to obtain the best correlation between TEI, SEI and BEI.

Results

Bottom SED examination

Thin sections. Images by SED of thin sections (ST 80 nm) provide similar information as those obtained by TEM. Fig. 1a is an SEI(-) from a human carotid artery conventionally stained. Some smooth muscle cells, embedded in an extracellular matrix, are clearly recognized. Fig. 1b shows a smooth muscle cell in detail. Focal densities (FD) of actin as well as the external lamina (EL) are well imaged. The circle shows some collagen fibrils in the matrix.

Fig. 2 refers to a human myocardium section, conventionally stained and subjected to an immuno-gold procedure in order to visualize actin. Well correlated 4 kV SEI(-) (Fig. 2a) and 15 kV SEI(-) (Fig. 2b) were obtained thus providing a better evaluation of the surface reaction. The 15 kV SEI(-) shows the more defined distribution of gold particles (GP).

Fig. 1. Section collected on grid of a human carotid artery. Uranyl acetate and lead citrate stains. FD: focal densities; EL: external lamina; circle: collagen fibrils.
ST 80 nm. PE 5 kV. S 20 nm.

Fig. 2. Section collected on grid of a human myocardium, conventionally stained and subjected to an immuno-gold procedure in order to visualize actin. GP: gold particles.
ST 80 nm. PE (a) 4 kV; (b) 15 kV. S 20 nm.
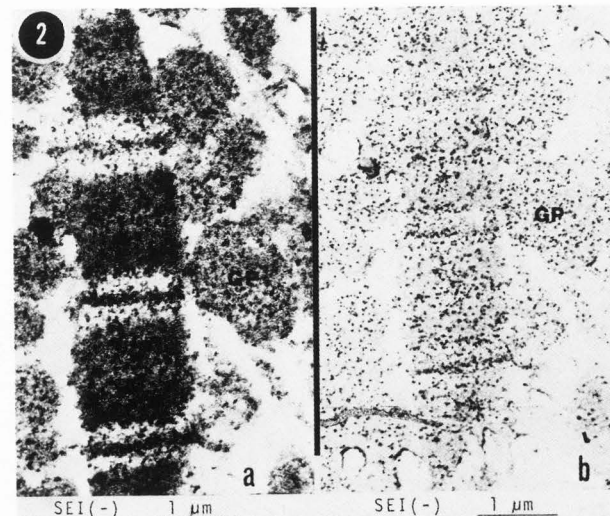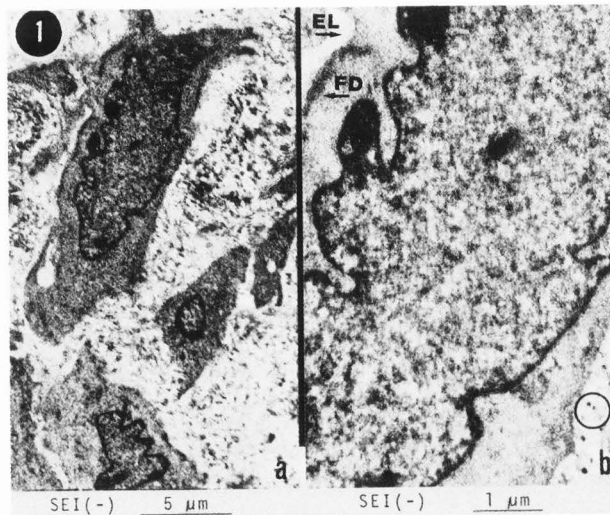
Semithin sections. Examination by SED of semithin sections (ST 0.5-1 µm) provides complementary images in contrast with those obtained in BSE mode. Moreover, information related to different layers of the section can be imaged, by varying the PE voltages.

Figs. 3 and 4 refer to a section of human carotid artery, collected on glass and presenting a whole thickness staining (tannic acid and osmium tetroxide impregnation) associated to a conventional one. At 15 kV, the SEI(-) (Fig. 3a) provides information on the internal high Z structures of the samples. Subsurface information is predominant because of generated BSE in the depth of the specimen. Note the elastic fiber arrangement (EF) and the nuclear morphology (N) of a smooth muscle cell.
By reducing the beam voltage (PE 2 kV), surface details are imaged (see the knife marks, arrows, Fig. 3b). This effect most likely depends on the fact that there is an increase in SE emission, at low PE values. Moreover, for low PE, the area of the section, from which SE-II are emitted is small. By comparing Figs. 3a and 3b, it can be seen that subsurface structures (EF, N) are better defined in Fig. 3b. In fact, a low PE improves the contrast of the section by cancelling the unwanted BSE generated at the glass substrate (background signal). SEI(-) taken at 1 kV (Fig. 4a) and 0.6 kV (Fig. 4b) show a clear decrease in the signal to noise ratio due to the low incident beam current. Contrast from internal high Z areas is weak in Fig. 4a and absent in Fig. 4b. Surface defects are also not clearly imaged.

Figs. 5 and 6 are from a small intestine section collected on grid, subjected to an immunocytochemical surface reaction with high Z elements (Ag, Au) and conventionally stained. At 15 kV, the SEI(-) (Fig. 5a) shows information from both the internal high Z areas (nuclear morphology, N) and the surface high Z reaction (surface reaction, SR). At the same time, the grid bar (GB), located 1 µm below the surface section, is still imaged.
For 10 kV (Fig. 5b), a better resolved SEI(-) is obtained. Single gold particles are seen; the nuclei are well defined. Moreover, the contrast from the grid bar is totally absent because of the strong dependence of signal depth on the beam voltage.
At 2 kV, the SEI(-) (Fig. 6a) allows to discriminate the surface contrast from the subsurface one. Note the absence of nuclear details. After a further reduction of PE (0.6 kV), SEI(-) (Fig. 6b) shows a low signal to noise ratio, even though a topographic contrast is visualized. Microfolds are well imaged where the section

adheres to the grid bar (arrows).
Since a "true" topographic contrast increases with metal coating (Peters, 1979), a thin film of gold (20 nm) was deposited onto the small intestine section. At 2 kV (Fig.7), microfolds (arrows) are more pronounced and edge contrast becomes apparent.Compare to Fig. 6a.

Top SED examination

Thin sections. Samples, similar to those previously viewed at SEM, were observed by a top SED in STEM.
Fig. 8 refers to a human kidney section conventionally stained and presenting on its surface randomly distributed gold particles (20 nm and 40 nm mean diameters). Fig. 8a is a bright field TEI taken at 80 kV, with a 5 nm beam spot size. TEI does not permit to discriminate internal high Z structures (i.e. nucleolus, NU) from surface high Z particles (i.e. gold particles, GP). Fig. 8b shows the same area in SE(+) mode. In this image, only the gold particles are visualized. Internal features lack in contrast. By comparing Fig. 8a to Fig. 8b, it can be seen that gold particles in SEI are larger than those imaged in TEI.

Fig. 3. Section collected on glass of a human carotid artery. Tannic acid-osmium tetroxide, uranyl acetate and lead citrate stains. EF: elastic fibers; N: nuclear morphology; arrows: knife marks. ST 1 µm. PE (a) 15 kV; (b) 2 kV; S 20 nm.

Fig. 4. The same field as seen in Fig. 3. EF: elastic fibers; N: nuclear morphology; arrows: knife marks.
ST 1 µm. PE (a) 1 kV; (b) 0.6 kV. S 20 nm.

Fig. 5. Section collected on grid of a human small intestine, conventionally stained and subjected to an immunocytochemical surface reaction with high Z elements (Ag, Au). N: nuclear morphology; SR: surface reaction; GB: grid bar.
ST 1 µm. PE (a) 15 kV; (b) 10 kV. S 20 nm.

Fig. 6. The same field as seen in Fig. 5. N: nuclear morphology; SR: surface reaction; arrows: microfolds. ST 1 µm. PE (a) 2 kV; (b) 0.6 kV. S 20 nm.

Fig. 7. The same section as seen in Figs. 5 and 6, but coated with a 20 nm of gold. SR: surface reaction; arrows: microfolds.
ST 1 µm. PE 2 kV. S 20 nm.

Fig. 8. Section collected on grid of a human kidney, conventionally stained and presenting on its surface randomly distributed gold particles. Nu: nucleolus; GP: gold particles.
ST 80 nm. PE 100 kV. S (a) 5 nm; (b) 20 nm.
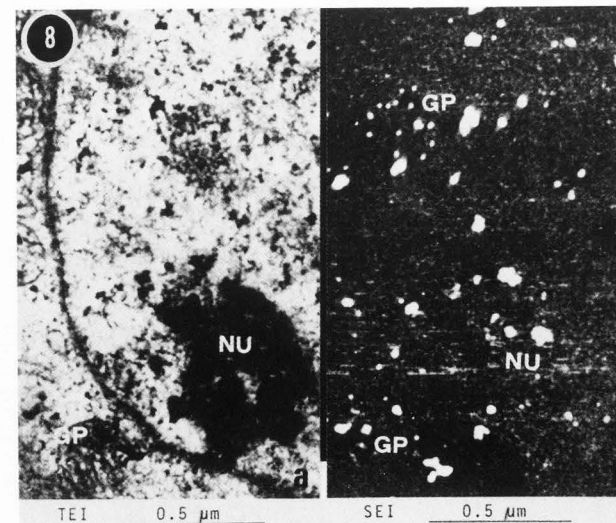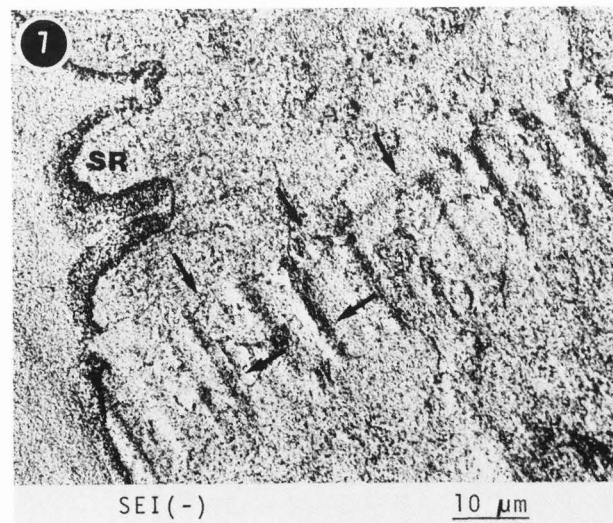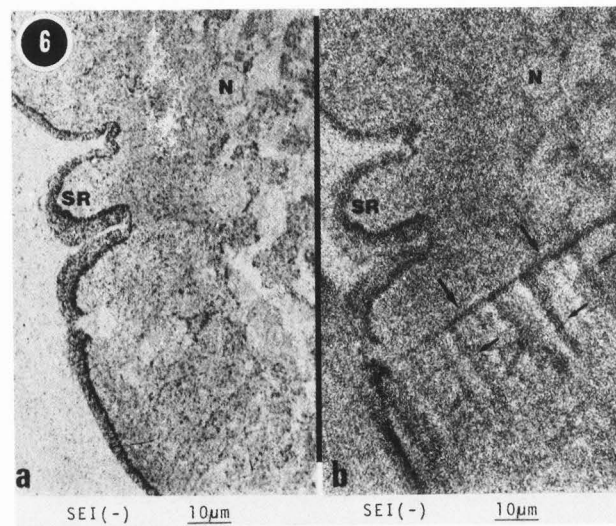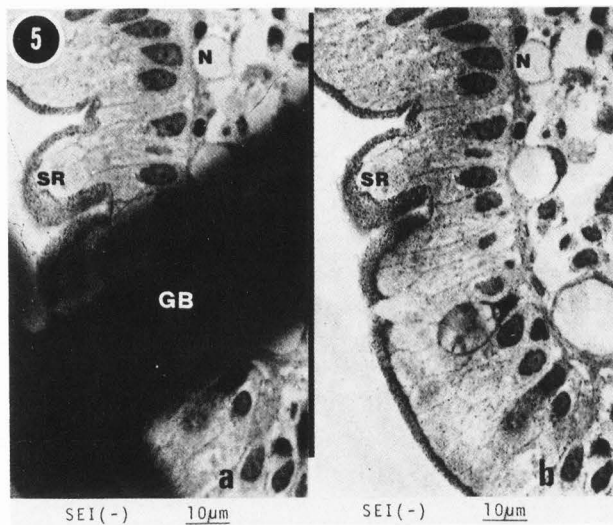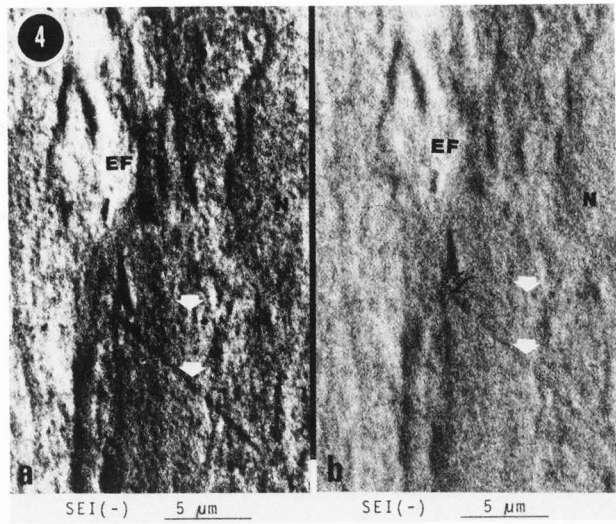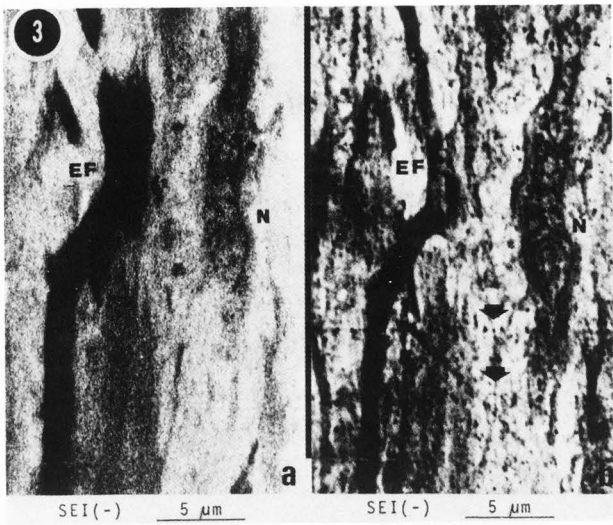
This depends on differences in the beam spot size while taking the two images (TEI, S 5 nm; SEI, S 20 nm). Moreover, since the nature of SEI changes with the size of the object (George and Robinson, 1976; Peters 1982a), for 20-40 nm gold particles backscattering may be large enough to give a substantial SE-II contribution to the final SE image. Therefore SEI resolution will be lowered.

Fig. 9 is the same human myocardium section examined at SEM (see Figs. 2a and 2b). TEI (Fig. 9a) shows some distinct sarcomeres (S). A homogeneous labelling (GP) is present on the bundles of actin filaments. However, SEI(+) (Fig. 9b) is necessary for better assessment of the surface reaction. The arrows show some edge effects related to etching defects of the section.

Semithin sections. In order to study how the specific components (SE-I, SE-II) of the signal collected by top SED affect SE resolution, a particular sample has been prepared. A kidney semithin section was collected on grid. Numerous gold particles (20 nm and 40 nm ranging in size) were randomly distributed on one side of the section (side A); the other one (side B) was conventionally stained with uranyl acetate and lead citrate.

Fig. 10 refers to the sample with side A towards the SED. In TE mode (Fig. 10a), internal features (i.e. foot processes, FP) and surface particles (gold particles, GP) were detected at the same time. Fig. 10b is an SEI(+) taken at the same beam voltage (100 kV) as TEI. High Z particles (GP), located at the top of the specimen, are viewed with good resolution, even though a weak internal contrast (FP) is still imaged. SEI(+) of the same field but at lower PE voltage (40 kV, Fig. 10c) shows only the surface gold particles. Resolution seems to be reduced. Vertical striations are instrument faults. The same sample was turned and observed with side B towards SED. As the internal morphology (M) and the gold particles (GP) are still imaged, TEI (Fig. 11a) supplies information similar to that obtained in Fig. 10a. Only gold particles are seen with poor resolution in SE(+) mode (Fig. 11b). This time, the SEI comes only from the SE-II component. BSE, originated from interaction between PE and gold particles, which are located below the section, are spread by multiple scattering within the specimen. Since they re-emerge at some distance from the PE entry point, the resulting SE-II provide delocalized information related to the high Z gold particles. The internal details (M) are not resolved due to an increase in the unwanted background.

The next example shows how the variation of PE may affect the information depth in STEM. We

Fig. 9. Section collected on grid of a human myocardium, conventionally stained and subjected to an immuno-gold procedure in order to visualize actin. S: sarcomeres; GP: gold particles; arrows: etching defects.
ST 80 nm. PE 100 kV. S (a) 5 nm; (b) 20 nm.

Fig. 10. Section collected on grid of a human kidney, conventionally stained and presenting on this surface gold particles (20 and 40 nm ranging in size). Side A towards the SED. FP: foot processes; GP: gold particles.
ST 0.5 μm. PE (a) 100 kV; (b) 100 kV; (c) 40 kV. S (a) 5 nm; (b) 20 nm; (c) 20 nm.

Fig. 11. The same section as seen in Fig. 10. Side B towards the SED. M: internal morphology. GP: gold particles.
ST 0.5 μm. PE 100 kV. S (a) 5 nm; (b) 20 nm.

Fig. 12. Section collected on grid of a human carotid artery. Tannic acid-osmium tetroxide, uranyl acetate and lead citrate stains. EF: elastic fibers; asterisk: low contrasted fibers.
ST 1 μm. PE 80 kV. S 20 nm.

Fig. 13. The same field as seen in Fig. 12. EF: elastic fibers; asterisk: low contrasted fibers; arrows: cutting defects.
ST 1 μm. PE (a) 80 kV; (b) 60 kV. S 20 nm.

Fig. 14. The same field as seen in Figs. 12 and 13. EF: elastic fibers; asterisk: low contrasted fibers; arrows: cutting defects.
ST 1 μm. PE (a) 40 kV; (b) 20 kV. S 20 nm.

---

observed the same semithin section of human carotid artery previously seen at SEM by the bottom SED (see Figs. 3 and 4). The same field was observed in TE (Fig. 12a), BSE(-) (Fig. 12b) and SE(-) (Fig. 13a) modes keeping constant the PE voltage (80 kV). TEI shows different elastic fibers, most likely located at different planes of the section. Some fibers present similar contrast (EF_1, EF_2), whereas others are imaged with a lower one (asterisk). The same type of information was obtained in BEI(-), even though the signal emitted from low contrasted areas is poor. Substantial differences in signal strength between EF_1 and EF_2 were only seen in SEI(-). Contrast from the central part of EF_1 is low and this may depend on its subsurface localization. EF_2, instead, present a homogeneous contrast in all the images examined. The arrangement of EF_2 is most likely next to the surface plane of the section. The low contrasted areas, viewed in TEI and BEI(-), are not imaged because of their deeper location. Moreover, some surface details, related to cutting defects, are viewed in SEI(-) (Fig. 13a, arrows).
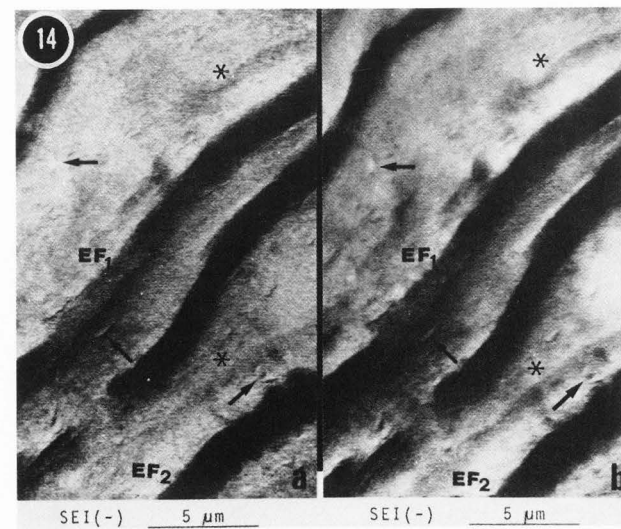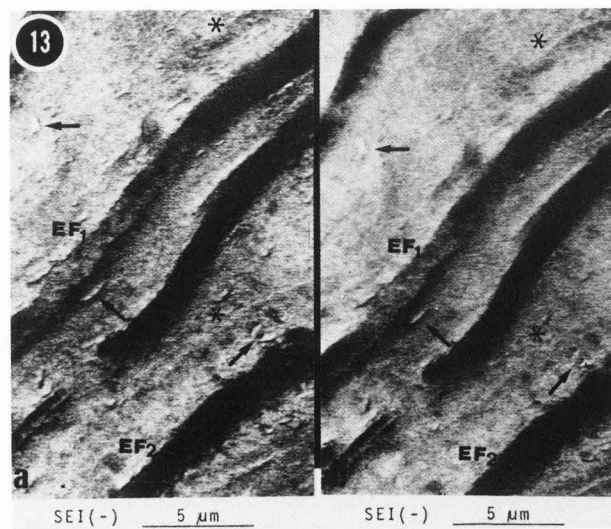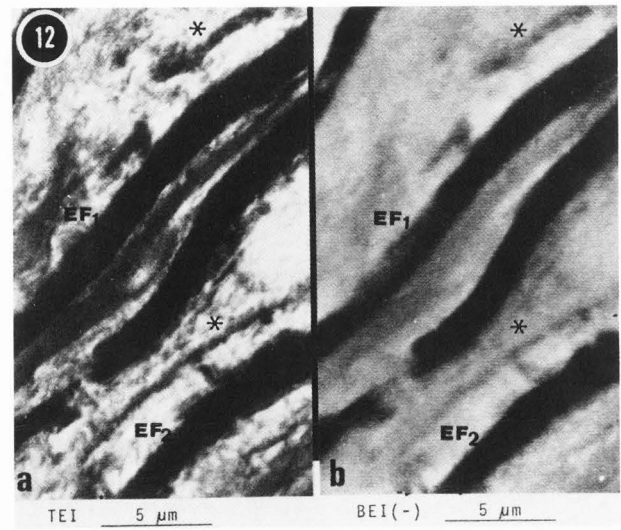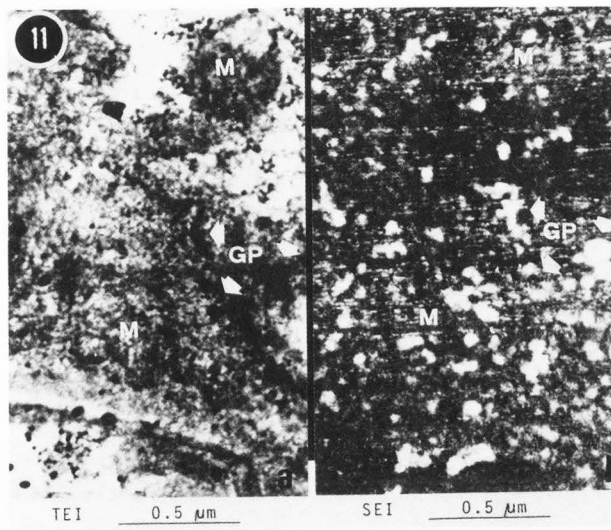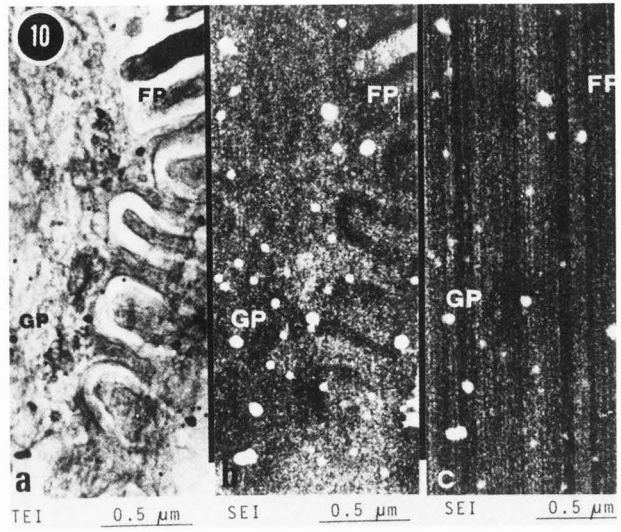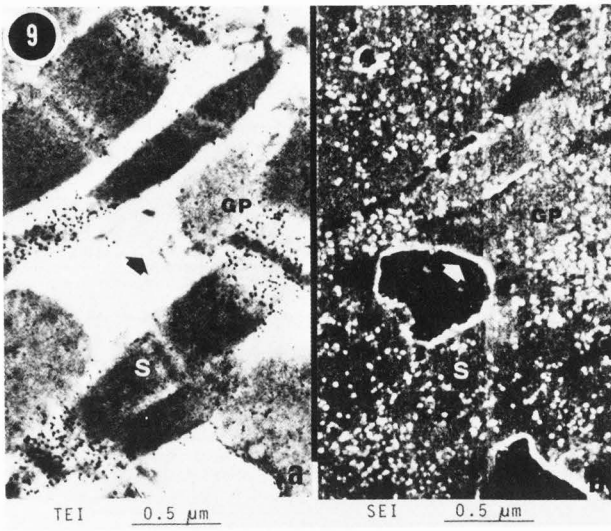
Figs.13b, 14a and 14b are SEI(-) imaged at different PE voltages (60, 40, 20 kV). By reducing the PE, the signal to noise ratio readily decreases thus making resolution poor. Contrast differences between EF_1 and EF_2 are attenuated and low contrasted areas are present again.

Monte Carlo simulation

Since Monte Carlo computation can be adapted to simulate any experimental situation of interest, we used this approach to study the way in which the physical properties of the metal coating affect the characterization of the information depth in the SE and BSE modes. Table 1 shows the results computed by the Monte Carlo program for high and low PE voltages in thin films (20 nm) of Au and C.
From this computation one can observe that information from different layers of the samples can be expected at different PE values. If metal films are deposited onto a biological specimen, both the film and the specimen can participate in the signal generation. For low PE (0.6 kV), our data show that the incident electrons do not pass through these metal layers. Thus, contrasts are generated by the metal films. As the beam voltage is changed from 30 to 80 kV, there is a progressive increase both in the TE generation and in the BSE emission. Moreover, BSE emission is strictly related to the specific metal atomic number (C, Z=6; Au, Z=79). Contrast can be now imaged from 20 nm below the surface of such metal films.

Conclusions

During the last few years, some authors have begun to use the SEM on sectioned biological material to correlate optical and ultrastructural information. Among the variety of electron induced signals which are produced in the SEM, the BSE signal attracted the attention of numerous authors for its strong dependence on specimen mean atomic number Z (Niedrig, 1978). For smooth specimens, such as sections, BSE provide images in which contrast is mainly proportional to the average Z of the sample (material contrast) but slightly related to topographic details (topographic contrast) (Reimer, 1976). Since examination of sectioned material has, so far, proven to be one of the most worthwhile biological applications of BSE, different methods of processing and staining material were tested with good results: semithin (0.5-1 μm), thick (more than 1 μm) sections of paraffin, plastic embedded material stained with heavy metal dyes (DeNee et al., 1977; Kushida et al., 1977; Dichiara et al., 1980; Ogura and Hasegawa, 1980; Ogura and Laudate, 1980; Hartman and Nakane, 1981).

TABLE 1.

MONTE CARLO THIN FILM
Thickness : 20 nm

CARBON			GOLD		
Electrons : 2007		VOLTAGE: 0.6 kV	Electrons : 2008		
BSE : 1			BSE : 1		
TE : 1			TE : 0		
Electrons : 786		VOLTAGE: 30 kV	Electrons : 301		
BSE : 0			BSE : 22		
TE : 786			TE : 279		
Electrons : 2014		VOLTAGE: 80 kV	Electrons : 2003		
BSE : 0			BSE : 12		
TE : 2014			TE : 1991		

Well contrasted and resolved BSE images were obtained thus permitting a close correlation between light microscopy and scanning electron microscopy images.

The SE signal, instead, has been extensively used for imaging the surface topography of conventional processed bulky specimens. In fact, three-dimensional fine structures of surfaces of biological specimens are easily visualized with SEM in SE mode (Pfefferkorn, 1975). The conventional bottom SED collects SE from various sources as well as BSE: SE produced both by the PE (SE-I) and by exiting BSE (SE-II, SE-III); BSE emitted towards the SED itself. Therefore, the total SE signal detected by SED is strongly BSE dependent (Reimer et al., 1968; Drescher et al., 1970; Peters, 1982b; Volbert, 1982; Hasselbach, et al., 1983).

We studied, by SED, thin and semithin sections of embedded biological material stained with cytochemical and immunocytochemical procedures (Pasquinelli et al., 1985; Scala et al., 1985). In this way, it was possible to detect by SED those electrons which re-emerge from the surface of a relatively thin specimen with little surface morphology. The resulting SE images were similar to those produced by the conventional transmission electron microscope, though generally with much poorer resolution. For such smooth specimens, the material contrast (BSE, SE-II, SE-III) was so large that SEI could be readily interpreted. However, a limited topographic contribution (SE-I, SE-II) was also evidenced because we were able to visualize some surface defects of the sections (i.e. knife marks). Furthermore, we considered some instrumental and

operating parameters affecting the final image produced by SED. Specimen resolution is mainly determined by the beam spot size; short working distances increase the resolution by reducing the spherical aberration of the final lens and the external magnetic field influence; tilting of the specimen affects the final SEI by changing the area excited and also by altering the zone of SE emission.

In this paper, different SE images were obtained from the same sample, by varying the PE voltages. Since specimen penetration of low voltage primary electrons is quite small, the surface contrast is imaged at low PE, whereas the subsurface one predominates at high PE. As discussed specifically by Pawley (1984) and Joy (1985), topographical information can be obtained by somehow separating the more localized SEI-I signal from the much larger SE-II and SE-III contribution, which is BSE dependent. This condition can be achieved on some biological specimens by coating the surface with ultra-thin (3-5 nm) metal films as suggested by Peters (1982b, 1983). His results, using a field emission SEM operated at high PE (30 kV), show a clear improvement of the topographical contrast over normal conditions. Another interesting approach involves reducing the PE (Thornley, 1960; Boyde, 1971; Catto and Smith, 1973; Pawley, 1984; Joy, 1985). For PE in the 1-5 kV range, the SE emission yield increases to unity and the electron range (R), which represents the SE distribution within the specimen, decreases. This means that the interaction between the PE and specimen is very localized. At low energies the SE-I is strictly related to the beam position and the SE-II has an R which is comparable with the SE escape range (8-10 nm): thus, the SE-I and SE-II contribution cannot be separated (Joy, 1985). As a consequence of this, the SE-I and SE-II signals provide information from the same area of the specimen corresponding to the SE escape depth. The resulting SEI should present a significantly greater topographical contrast. Fig. 5a is an SEI(-) taken at 15 kV. In this case, a material contrast is predominant (SE-II, SE-III). Note how these electrons are carrying information from a very deep volume of the section (grid bar). An SE-I contribution is not imaged. At 10 kV (Fig. 5b) the grid bar disappears but the main contrast mechanism is still a material one. In Fig. 6b (0.6 kV) a topographical contrast becomes apparent. Microfolds, which were not previously seen, are now well resolved. An acceptable signal to noise ratio is achieved, due to
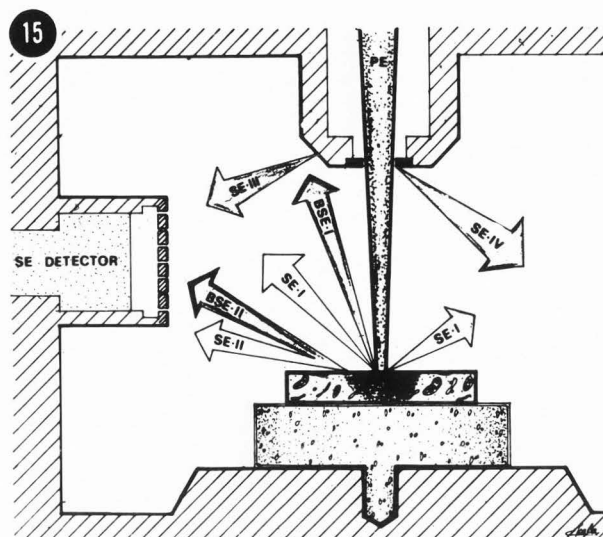
Fig. 15. Schematic view of bottom SED arrangement (conventional SEM). SE and BSE are both collected by SED.
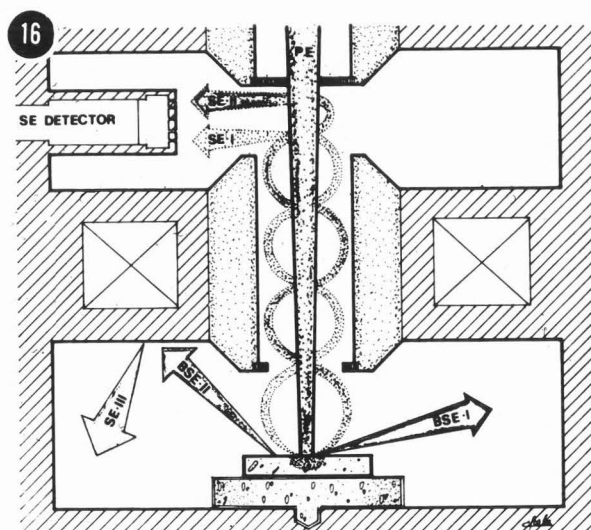

Fig. 16. Top SED location (STEM). The BSE contribution is minimized.

the use of the LaB$_6$ cathode. This cathode improves, in fact, the thermoionic gun brightness at low PE (Pawley, 1984). After coating with a thin metal layer, the same microfolds are evidenced with a greater contrast at 2 kV (Fig. 7). As for the material contrast, it is possible to

isolate SE images produced at different planes of the section as the PE penetration is changed. Using different SE images, one should be able to reconstruct a three-dimensional view of the section examined with an appropriate image analyzer. Moreover, SED is very effective in the examination of sections presenting surface immunocytochemical reactions with high Z elements. Gold particles are well visualized thus displaying antigens and receptors on sectioned tissue. Morphological features can also be imaged at the same time. Double labelling could be evidenced at different PE voltages, by using both high Z (i.e. colloidal gold) and particulate low Z (i.e. synthetic macromolecular particles) markers (see Molday and Maher, 1980 for an excellent review).

The signal contribution of metal coating to the final SEI should be now considered. Embedding media are insulators. This means that the epoxy resins are not, naturally, good conductors of electricity and heat. SEM examination is hindered by "charging" and "beam damage" effects. Coating specimens with a thin layer of a conductive material allows to overcome these problems. An additional advantage of metal coating is the improvement in the strength of the SE signal emitted from the specimen surface (Echlin, 1978). However, coating techniques are not yet optimal, i.e. "semithin" metal coatings can obscure surface details (Peters, 1979). Therefore, a Monte Carlo simulation for different PE voltages (0.6, 30, 80 kV) in thin (20 nm) films of Au and C was performed (Table 1). As for very low PE (0.6 kV), these films show similar properties. The incident electrons do not pass through the metal layer but remain close to the area of the entry point. Thus, a localized SE emission can be produced.
For high PE (30 kV), the Monte Carlo computation shows the typical progressive increase in BSE emission with increase in the metal atomic number.
A large SE-II, SE-III contribution is expected from such gold coating. Carbon, instead, gives a minimal BSE contribution, as the incident PE, passing through the layer, suffers mainly low angle inelastic scattering events. Thus, a thin layer of carbon seems to be the better compromise to analyze the information depth of our material .
At the highest energy (80 kV), there are no significant differences. In this case, the SE-II contribution can be eliminated by using ultrathin metal coatings as those proposed by Peters (1979, 1982b).
Finally, the collection geometries of SED may greatly affect the quality of the SEI. In a

conventional SEM, the signal collected by the bottom SED (Fig. 15) is partially BSE dependent whereas in STEM, as a consequence of the particular position of the SED (top detector, Fig. 16), located within the objective lens, the signal collected is formed mainly by SE-I and SE-II (Buchanan, 1983; Kawamoto et al., 1984; Pawley, 1984). By varying the PE in the 20-100 kV range, the SE images were better resolved at the highest PE (compare Fig. 13 to Fig. 14), even though the information remains the same. The degradation of the resolution of small surface details (see arrows) with decreasing energy seems attributable both to the spreading of the PE as it passes through the sample and to an increase in chromatic error.

In conclusion, as regards the PE variation, the bottom SED shows a greater versatility in the examination of embedded biological material.

Acknowledgements

References

Boyde A (1971). A review of problems of interpretation of the SEM image with special regards to methods of specimen preparation. Scanning Electron Microsc.1971: 1-8.

Buchanan R (1983). The scanning electron microscope for semiconductor application. Microelectronic Manufacturing and Testing, February,22-24.

Catto CJD, Smith KCA (1973). Resolution limits in the surface scanning electron microscope. J Microsc 98, 417-435.

Cotta-Pereira G, Guerra-Rodrigo F, David-Ferreira JF (1976). The use of tannic acid-glutaraldehyde in the study of elastic and elastic-related fibers. Stain Technol 51, 7-12.

Danscher G, Nörgaard IOR (1983). Light microscopic visualization of colloidal gold on resin-embedded tissue. J Histochem Cytochem 31, 1394-1398.

DeNee PB, Frederick RG, Pope RS (1977). Heavy metal staining of paraffin, epoxy and glycol methacrylate embedded biological tissue for Scanning Electron Microscope histology. Scanning Electron Microsc. 1977; II: 83-92.

Dichiara JF, Rowley PP, Ogilvie RW (1980). Back-scattered electron imaging (BEI) of paraffin sections stained with heavy metal histopathologic stains, with observations of some variables encountered in BEI. Scanning Electron Microsc. 1980; III: 181-188.

Drescher H, Reimer L, Seidel H (1970). Rucks-trenkoeffizient und Sekundarelektronen-Ausbeute von 10-100 KeV Elektronen und Beziehungen zur Raster-Elektronenmikroskopie. Z angew Phys 29, 331-336.

Echlin P (1978). Coating techniques for scanning electron microscopy and X-ray microanalysis. Scanning Electron Microsc.1978; I: 109-132.

Everhart TE, Wells OC, Oatley CW (1959). Factors affecting contrast and resolution in the scanning electron microscope. J Electron Control 7, 97-111.

Everhart TE, Thornley RFM (1960). Wide-band detector for micro-microampere low-energy electron currents. J Sci Instrum 37, 246-248.

George EP, Robinson VNE (1976). The dependence of SEM contrast upon electron penetration. Scanning Electron Microsc.1976; I: 17-26.

Hartman AL, Nakane PK (1981). Intracellular localization of antigens with backscatter mode of SEM using peroxidase-labeled antibodies. Scanning Electron Microsc.1981; II: 33-44.

Hasselbach F, Rieke U, Straub M (1983). An imaging secondary electron detector for the scanning electron microscope. Scanning Electron Microsc.1983; II: 467-478.

Joy DC (1984). Beam interactions, contrast and resolution in the SEM. J Microsc 136, 241-258.

Joy DC (1985). Resolution in low voltage scanning electron microscopy. J Microsc 140, 283-292.

Kawamoto H, Yamazaki S, Ishikawa A, Buchanan R (1984). Effects of secondary electron detector position on scanning electron microscope image. Scanning Electron Microsc.1984; I: 15-22.

Kushida T, Nagato Y, Kushida H (1977). Observation on the same place in semithin section with both light and electron microscopy. J Electron Microsc 26, 345-348.

McLean IW, Nakane PK (1974). Periodate-lysine-paraformaldehyde fixative: a new fixative for immunoelectron microscopy. J Histochem Cytochem 22, 1077-1083.

Molday RS, Maher P (1980). A review of cell surface markers and labelling techniques for scanning electron microscopy. Histochem J 12, 273-315.

Niedrig H (1978). Physical background of electron backscattering. Scanning 1, 17-34.

Oatley CW, Nixon WC, Pease RFW (1965). Scanning electron microscopy. In: Advances in Electronics and Electron Physics, pp. 181-247. Academic Press, New York.

Ogura K, Hasegawa Y (1980). Application of back-scattered electron image to biological specimen. J Electron Microsc 29, 68-71.

Ogura K, Laudate A (1980). Comparative observation with a light microscope and an SEM in backscattered electron mode. Scanning Electron Microsc.1980; I: 233-238.

Pasquinelli G, Scala C, Borsetti GP, Martegani F, Laschi R (1985). A new approach for studying semithin sections of human pathological material: intermicroscopic correlation between light microscopy and scanning electron microscopy. Scanning Electron Microsc.1985; III: 1133-1142.

Pawley J (1984). Low voltage scanning electron microscopy. J Microsc 136, 45-68.

Peters K-R (1979). Scanning electron microscopy at macromolecular resolution in low energy mode on biological specimens coated with ultra thin metal films. Scanning Electron Microsc.1979; II: 133-148.

Peters K-R (1982a). Validation of George and Robinson SE-I signal theorem. Proc. 40th Ann. Proc. EMSA (Ed. by Bailey GW) p.368. Claitors Press, Baton Rouge.

Peters K-R (1982b). Conditions required for high quality high magnification images in secondary electron-I SEM. Scanning Electron Microsc.1982; IV: 1359-1372.

Peters K-R (1983). Generation and properties of an SE-I enriched signal. In: Electron Beam Interactions with Solids. (Eds.) D.F. Kyser et al., SEM, Inc., AMF O'Hare, IL. 363-372.

Pfefferkorn G (1975). Introduction to scanning electron microscopy. Scanning Electron Microsc. 1975: 631-644.

Reimer L (1976). Electron specimen interactions and applications in SEM and STEM. Scanning Electron Microsc.1976; I: 1-8.

Reimer L (1979). Electron-specimen interactions. Scanning Electron Microsc.1979; II: 111-124.

Reimer L, Seidel H, Gilde H (1968). Einfluss der Elektronendiffusion auf die Bildentstehung im Raster-Elektronenmikroskop.Beitr. elektr. mikr. Direktabb. Oberfl. 1, 53-65.

Roth J, Bendayan M, Orci L (1978). Ultrastructural localization of intracellular antigens by the use of protein A-gold complex. J Histochem Cytochem 26, 1074-1081.

Scala C., Pasquinelli G, Martegani F, Laschi R (1985). Use of secondary electron detectors for compositional studies on embedded biological material. Scanning Electron Microsc.1985; IV: 1709-1718.

Thornley RFM (1960). Recent developments in scanning electron microscopy. In: Proc. Eur. Reg. Conf. Electr. Microsc. Delft (Ed. by Houwink Al. and Spit BJ) pp. 173-176.

Volbert B (1982). Signal mixing techniques in scanning electron microscopy. Scanning Electron Microsc.1982; III: 897-905.

Discussion with Reviewers

K.-R. Peters: Which scattering models were used to calculate or estimate the increase of SE-I emission at 0.6 kV?

Authors: We used the model by Joy on Monte Carlo calculations of electron scattering in solid samples at different voltages (Joy, 1985).

K.-R. Peters: What ratio of SE-I and SE-II is expected at low kV of 0.6 kV?

Authors: Even though several computations have been proposed to calculate the yield of secondaries, the measurement of SE-I/SE-II ratio is still complex, especially at very low PE. However, Joy has shown a 3/1 ratio (SE-I/SE-II) on a bulk sample of carbon (paper reviewed in text, Joy, 1985).

K.-R. Peters: There are different definitions used for SE types. How large (in nm^2) is the exit surface area of SE electrons you designate as SE-I?

Authors: The SE-I are those SE which are directly generated by the incident electrons. The SE-I exitation volume is strictly located close to the beam axis and extends a few nm from the surface into the sample. This means that the SE-I signal is a function of the beam position and provides localized information about the specimen surface. Since the surface distribution of SE-I is slightly affected by the beam voltage, their exit area can be estimated only a few nm in diameter.

K.-R. Peters: Which SE signal type -- as you define it -- dominates contrasts of surface images obtained from 20 nm thick Au coatings?

Authors: The type II signal (SE-II).

K.-R. Peters: Topographic contrasts produced at low accelerating voltage before (Fig. 6) and after Au application (Fig. 7) are similar. Would this imply that the signal types, generating these contrasts, remain uneffected?

Authors: The total secondary yield δ total can be written as- δ total $= \delta$ SE-I. $(1 + \beta \eta)$- where η is the backscattering coefficient for the material and β is the factor of secondary production from BSE. As the beam voltage is reduced in the range 3-1 kV, the secondary yield rises rapidly in all materials, while η and β both remain essentially constant with beam energy. Moreover, the computed electron range (R) shows a rapid fall as a function of beam energy $(R = K V_o^{1.5})$ (Pawley, 1984; Joy, 1985). As a consequence of this, the SE-I and SE-II signals can be considered indistinguishable at very low PE. Thus, SE-I and SE-II provide information about the same region of the specimen when R is comparable with the SE escape depth. The resulting images will be better contrasted. In our case (Figs. 6 and 7), microfolds were evidenced before and after Au deposition, but Fig. 7 (Au coating) shows a greater contrast. We think that both the two images are due to the mechanisms discussed above (the topographic features are resolved in both the SE-I and the SE-II components).
However, as the backscattering coefficient varies monotonically with the atomic number of the target, a greater contrast (due to the increase in the type II component) is expected from a Au coated specimen.

J.B. Pawley: You have treated contrast of various types as a function of PE. Can you comment on resolution as a function of depth below the surface at the higher voltage?

Authors: At high energy, SED examination of biological sections provides images which are mainly BSE dependent. The BSE penetrate to a significant extent into the specimen before being scattered back to the surface. This property can be used in biological observation of sections where a specific high Z stain is used to decorate structures of interest. The possibility of obtaining subsurface information depends on the fact that the BSE coefficient η is strictly related to the Z of the target. Moreover, a sufficient energy must be used to hit the target itself. The spatial resolution of our images (semithin sections) is determined by the area over which the type II signal (BSE-II, SE-II) emerge from the surface. The diameter of BSE exit area is about 1/3 of R. The electron range is due to both the atomic number of the target and the beam energy. Computed data have demonstrated that R rises as the beam voltage is increased. An inverse correlation exists between R and Z. Thus, subsurface resolution (type II signals) is expected to be poor at high energy.